Supplement of Hydrol. Earth Syst. Sci., 30, 6983–7005, 2026
https://doi.org/10.5194/hess-30-6983-2026-supplement
© Author(s) 2026. CC BY 4.0 License.



Hydrology and Earth System Sciences
Open Access
EGU

Supplement of

Extreme glacier melt on the Central Tibetan Plateau during the summer of 2022: detection and mechanisms

Fei Zhu et al.

Correspondence to: Meilin Zhu (zhuml@lzu.edu.cn)

The copyright of individual parts of the supplement might differ from the article licence.

Table S1. List of the model parameters, range of parameters used to estimate the uncertainties in melt during extreme heat events and mass balance on Sangqu Glacier at glacier scale.

parameter	+/-	Sensitivity in melt (mm w.e.)
a_{snow}	0.03	61.7
a_{firn}	0.03	20.9
a	10%	0
b	10%	32.1
$T_{snow/rain}$(℃)	10%	0.6
P(%/100m)	10%	-1.9
C_b	10%	-6.1
K	10%	-21.8
S_{in}_K	0.01	-5.1
T_lapse_rate (℃/100m)	0.1	-63.6
E_k	10%	-9.9
C_{eff}	10%	10.5

Table S2. List of the model parameters, range of parameters used to estimate the uncertainties in mass balance during 2019/20 on Sangqu Glacier at glacier scale.

parameter	+/-	Sensitivity in mass balance (mm w.e.)
a_{snow}	0.03	124.1
a_{firn}	0.03	117.1
a	10%	-1.4
b	10%	77.8
$T_{snow/rain}$(℃)	10%	-0.3
P(%/100m)	10%	-7.3
C_b	10%	6.4
K	10%	-38.6
S_{in}_K	0.01	-15.4
T_lapse_rate (℃/100m)	0.1	-126.6
E_k	10%	-6.3
C_{eff}	10%	6.5

Table S3. List of the model parameters, range of parameters used to estimate the uncertainties in mass balance during 2020/21 on Sangqu Glacier at glacier scale.

parameter	+/-	Sensitivity in mass balance (mm w.e.)
a_{snow}	0.03	113.5
a_{firn}	0.03	133.8
a	10%	-0.4
b	10%	183.7
$T_{snow/rain}$(℃)	10%	1.8
P(%/100m)	10%	2.2
C_b	10%	22.7
K	10%	-57.9
S_{in}_K	0.01	-28.5
T_lapse_rate (℃/100m)	0.1	-134.2
E_k	10%	-14.6
C_{eff}	10%	14.2

Table S4. List of the model parameters, range of parameters used to estimate the uncertainties in mass balance during 2021/22 on Sangqu Glacier at glacier scale.

parameter	+/-	Sensitivity in mass balance (mm w.e.)
a_{snow}	0.03	132
a_{firn}	0.03	93.3
a	10%	0.8
b	10%	117.4
$T_{snow/rain}$(℃)	10%	-0.2
P(%/100m)	10%	-1.4
C_b	10%	-4.2
K	10%	-68.4
S_{in}_K	0.01	-16.9
T_lapse_rate (℃/100m)	0.1	-163.3
E_k	10%	-9.9
C_{eff}	10%	10.5

K is turbulent flux coefficient. C_b is background turbulent exchange coefficient. S_{in}_K is a constant, for which values are typically in the range 0.87–1.00, depending on the geographic position. E_k is effective thermal conductivity. C_{eff} is heat capacity.

Table S5. June–August S_{HI} and circulation indices for 2020–2022

Year	S_{HI} (ERA5)	SHI(tuotuohe)	GTI	NSI
2020	1.67	-	−1.25	−0.03
2021	1.86	1.29	0.36	0.24
2022	1.78	1.68	-0.12	2.12

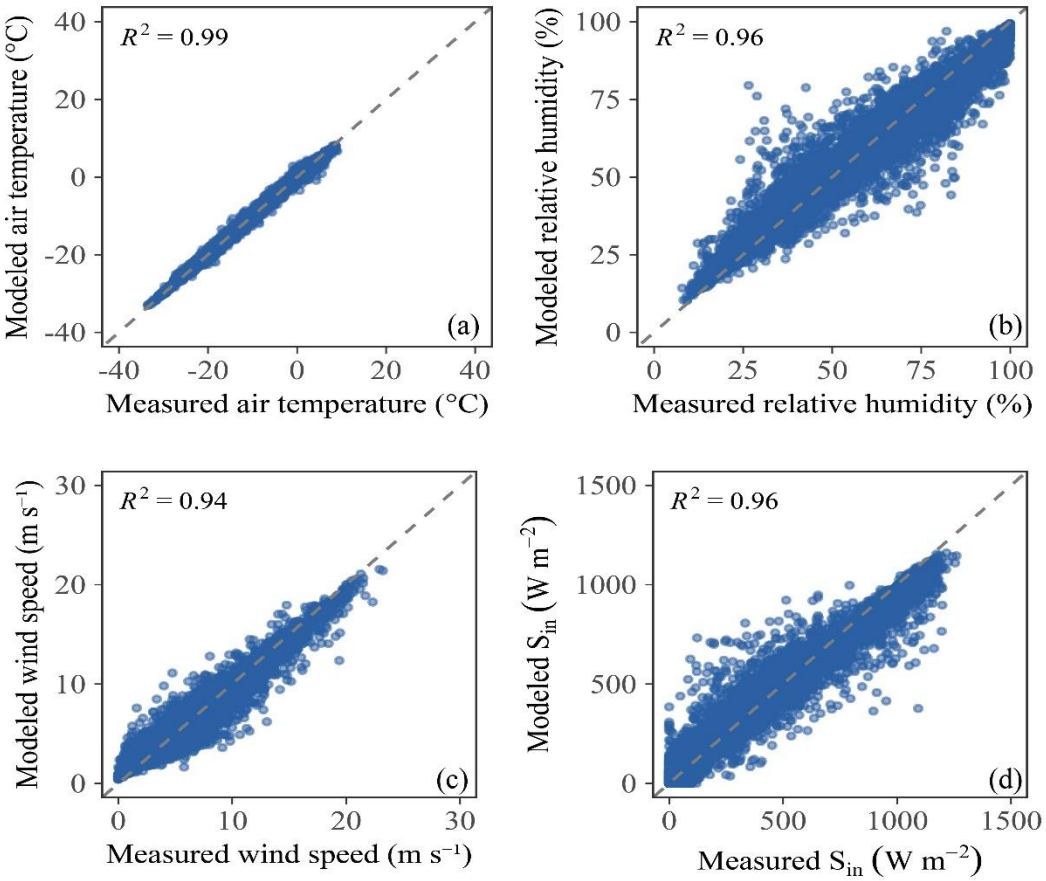
Note: Negative GTI indicates weaker westerlies; positive NSI indicates northward displacement of the SAH.

Table S6. Contributions of individual energy balance components to the +28.2 W m^{-2} melt energy anomaly during the three identified 2022 summer heatwave windows, relative to the October 2019–September 2021 reference period. Percentages may not sum to 100% due to rounding.

Component	ΔComponent (W/m^2)	ΔQ_M Contribution (W/m^2)	Percent (%)
L_{in}	20.3	+20.3	72.0
Q_H	17.0	+17.0	60.3
S_{out}	−8	+8	28.4
Q_G	−3.1	−3.1	−11
S_{in}	−2.9	−2.9	−10.3
Q_L	−4.8	−4.8	−17.0
L_{out}	+6.3	−6.3	−22.3

Table S7. Net contributions of energy balance components to the +28.2 W m^{-2} melt energy anomaly during the three identified 2022 summer heatwave windows, relative to the October 2019–September 2021 reference period. Percentages may not sum to 100% due to rounding.

Component	ΔComponent (W/m^2)	ΔQ_M Contribution (W/m^2)	Percent (%)
Q_H	17.0	17	60.3
L_{net}	14.0	14	49.7
S_{net}	+5.1	5.1	18.1
Q_G	−3.1	−3.1	−11
Q_L	−4.8	−4.8	−17.0

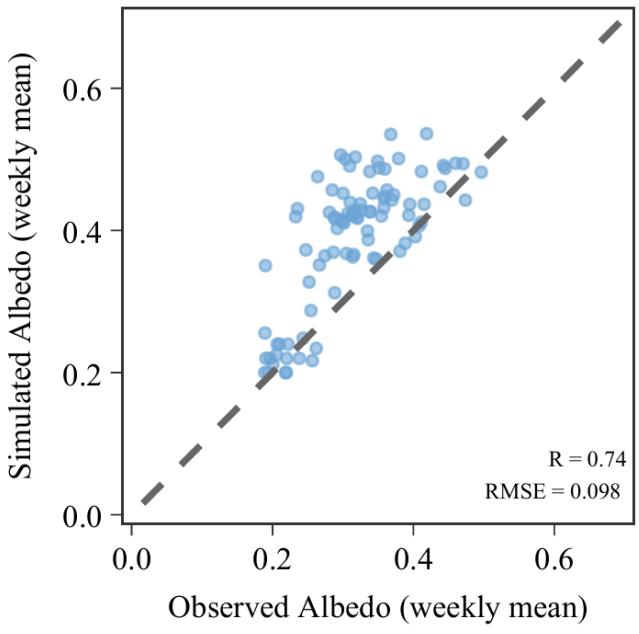


49

50 **Figure S1.** Comparison of observed and ERA5 downscaled (a) Air temperature, (b) Relative

51 humidity, (c) Wind speed, and (d) Incoming shortwave radiation at the hourly scale.

52



53

Figure S2. Comparison of albedo at weekly scale at the AWS site on Sangqu Glacier.

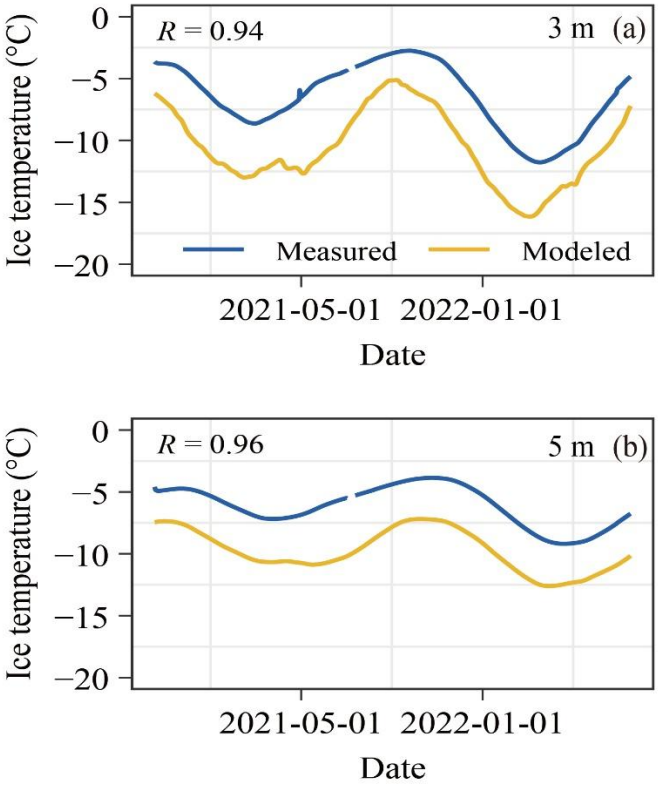


Figure S3. Comparison of observed and simulated ice temperatures at (a) 3 m and (b) 5 m.

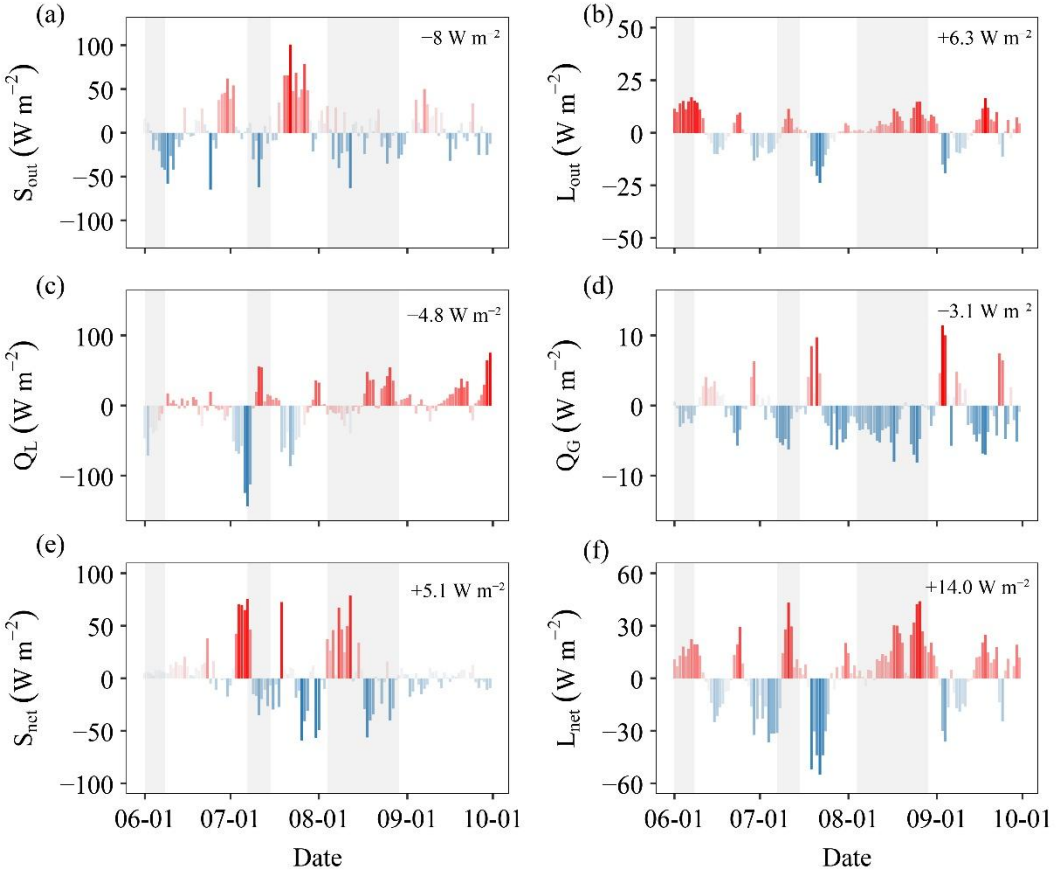


Figure S4. Glacier-wide energy balance anomalies associated with the extreme melt events. Anomalies in (a) outgoing shortwave radiation, (b) outgoing longwave radiation, (c) latent heat flux, (d) snow/ice heat flux, (e) net shortwave radiation, and (f) net longwave radiation are shown relative to the average of the June–September periods in 2019, 2020, and 2021. Gray shading indicates the three identified 2022 heatwave windows. The anomalies refer to these heatwave windows, not the entire June–September period.

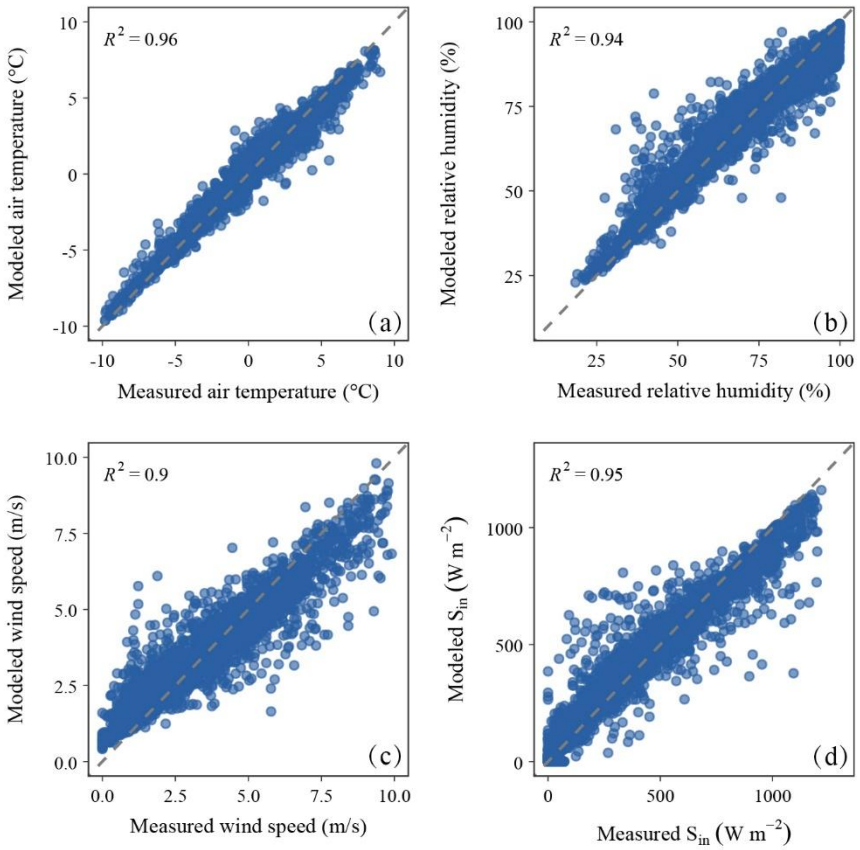


Figure S5. Comparison of observed and ERA5 downscaled (a) air temperature, (b) relative humidity, (c) wind speed, and (d) incoming shortwave radiation at the hourly scale during the ablation season (June–September).

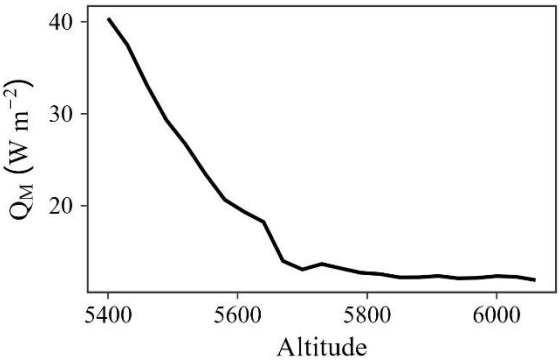


Figure S6. Melt energy versus elevation for the 2021–2022 mass balance year.

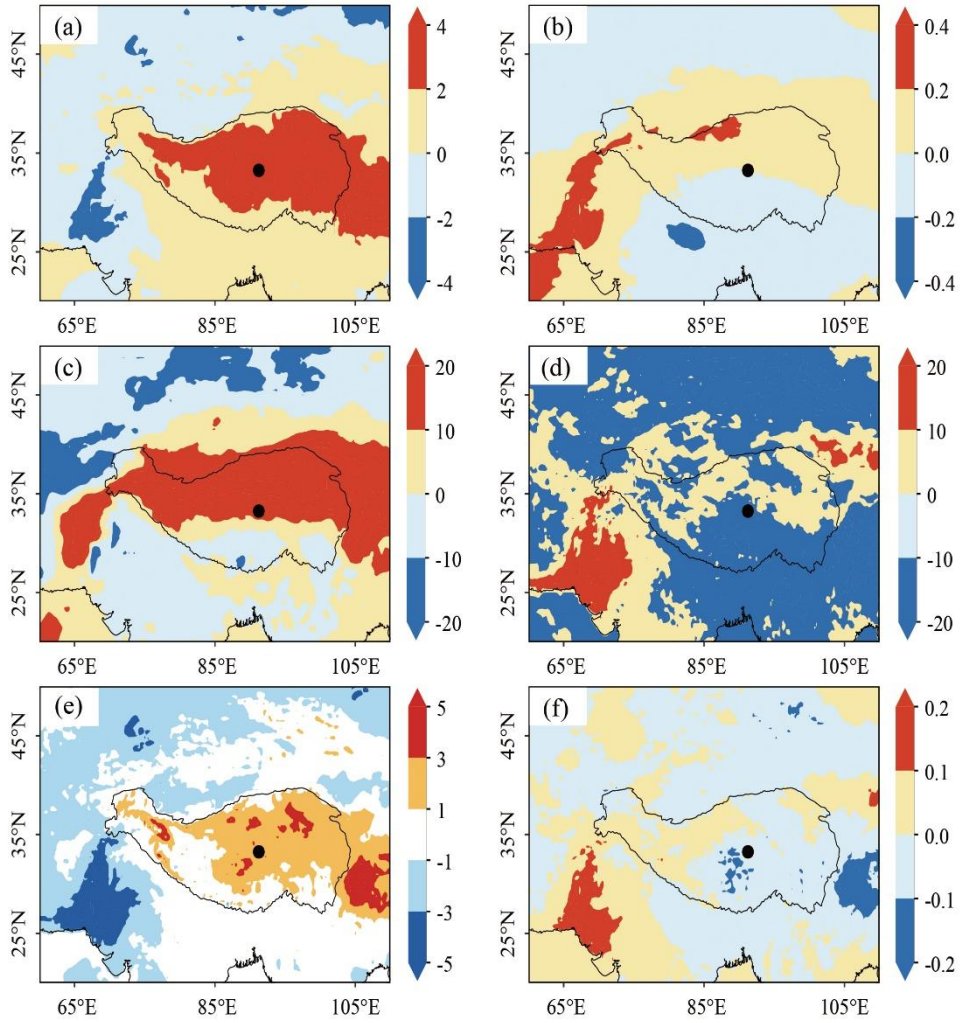


Figure S7. Anomalies in (a) air temperature (K), (b) cloud cover, (c) incoming longwave radiation (W/m^2), (d) sensible heat flux (W/m^2), (e) soil temperature (K), and (f) soil moisture ($m^3\ m^{-3}$) during the summer 2022 heatwave (reference period: 1992–2021).

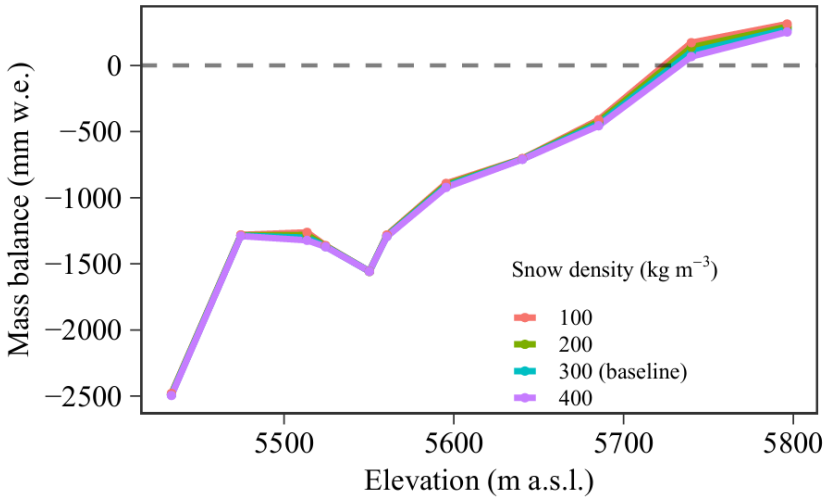


Figure S8. Sensitivity of point mass balance to snow density at different elevations for the 2019/20 mass balance year.

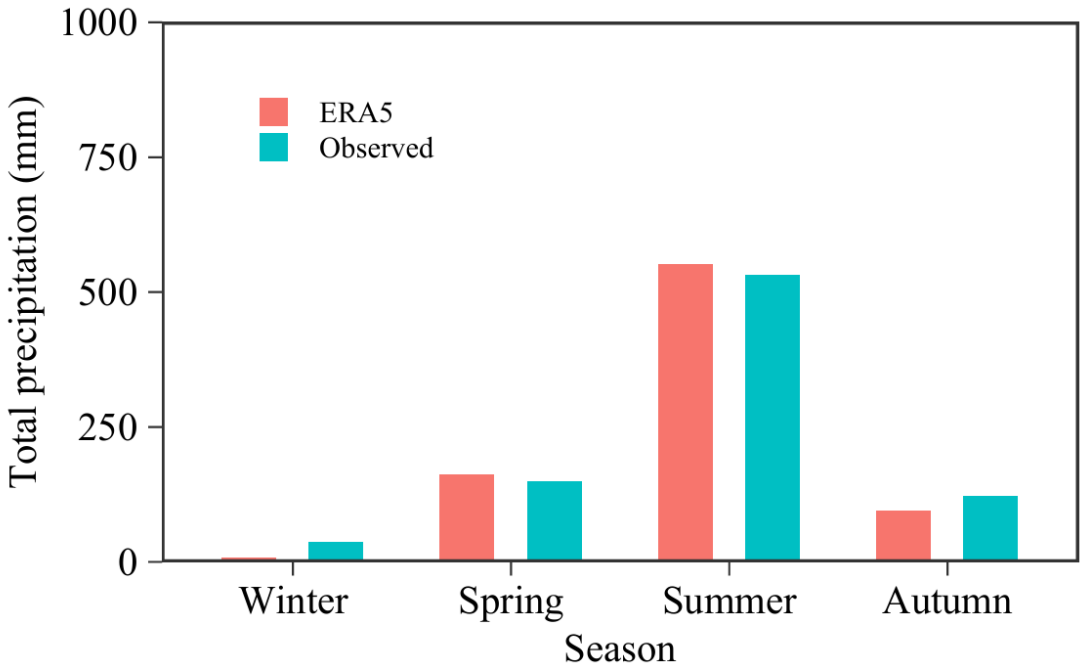


Figure S9. Seasonal comparison between ERA5 and in-situ precipitation measurements at Sangqu Glacier.